Nanoscale

PAPER

View Article Online
View Journal | View Issue

Cite this: *Nanoscale*, 2024, **16**, 2409

Investigating the effects of the local environment on bottlebrush conformations using super-resolution microscopy†

Jonathan M. Chan, Avram C. Kordon and Muzhou Wang *

The single-chain physics of bottlebrush polymers plays a key role in their macroscopic properties. Although efforts have been made to understand the behavior of single isolated bottlebrushes, studies on their behavior in crowded, application-relevant environments have been insufficient due to limitations in characterization techniques. Here, we use single-molecule localization microscopy (SMLM) to study the conformations of individual bottlebrush polymers by direct imaging. Our previous work focused on bottlebrushes in a matrix of linear polymers, where our observations suggested that their behavior was largely influenced by an entropic incompatibility between the bottlebrush side chains and the linear matrix. Instead, here we focus on systems where this effect is reduced: in solvent-swollen polymer materials and in systems entirely composed of bottlebrushes. We measure chain conformations and rigidity using persistence length (l_p) as side chain molecular weight (M_{sc}) is varied. Compared to a system of linear polymers, we observe greater flexibility of the backbone in both systems. For bottlebrushes in bottlebrush matrices, we additionally observed a scaling relationship between l_p and M_{sc} that more closely follows theoretical predictions. For the more flexible chains in both systems, we reach the edge of our resolution limit and cannot visualize the entire contour of every chain. We bypass this limitation by discussing the aspect ratios of the features within the super-resolution images.

Received 5th October 2023,
Accepted 20th December 2023

DOI: 10.1039/d3nr05000a

rsc.li/nanoscale

Department of Chemical and Biological Engineering, Northwestern University, Evanston, Illinois 60208, USA. E-mail: mwang@northwestern.edu

†Electronic supplementary information (ESI) available. See DOI: https://doi.org/10.1039/d3nr05000a

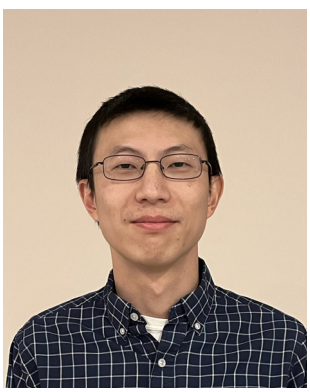

Muzhou Wang

Muzhou Wang is an associate professor in the Department of Chemical and Biological Engineering at Northwestern University, where he leads a group with interests including polymer self-assembly and physics, biomimetic materials, and optics. He was previously a postdoctoral fellow at the NIST, where he worked with Drs. Jeffrey W. Gilman and J. Alexander Liddle. His Ph.D. is in chemical engineering from MIT, under the supervision of Prof. Bradley D. Olsen. His work has been recognized with several awards including an NSF CAREER award, an Alfred P. Sloan Fellowship, and the Camille Dreyfus Teacher-Scholar Award.

Introduction

Bottlebrush polymers have applications in a wide range of fields, including electronics,[1,2] biomedical materials,[3–6] additive manufacturing,[7,8] and recyclable materials.[9] Often, these applications utilize bottlebrush polymers in crowded systems such as bulk materials or concentrated solutions, where the behavior of individual chains within a field of neighboring chains determines many of the resulting properties. For example, the soft mechanical properties of bottlebrush elastomers arise from their rigid conformations that result in decreased entanglements.[4] In another example, concentrated polymer solutions exhibit unique flow properties, such as low entanglements and strain hardening due to side chain interactions.[10–14] A deeper understanding of single-chain physics in crowded environments would enable better materials design for a myriad of applications.

In crowded environments, our knowledge of bottlebrush behavior has been limited. For dilute solutions, small-angle neutron scattering has revealed both transitions between globule- and rod-like geometries at different molecular architectural regimes as well as a concentration dependence of

polymer size and rigidity.[10,15,16] However, these studies are often limited to concentrations below those found in most applications, such as inks for additive manufacturing.[7] While studying solid bottlebrush materials, scattering techniques have also revealed that backbones possess higher degrees of rigidity depending on their position within the self-assembled structures of multiblock systems.[17,18] However, because scattering is indirect and requires model fitting, it is difficult to reveal details about single polymer chains. Helium ion microscopy is a powerful imaging technique that has been applied to bulk bottlebrush systems, and studies utilizing this method have revealed phenomena such as liquid crystal-like chain alignment in annealed samples. However, this surface-specific technique may not accurately characterize the behavior within the bulk of a material.[19] Instead, single-molecule localization microscopy (SMLM) has the ability to probe within crowded systems and shows great promise in studying single bottlebrushes to understand their single chain behavior.[20,21]

Previously, we have used SMLM to study bottlebrushes dispersed within a solid matrix composed of linear polymers.[22,23] These studies proved inadequate for investigating bottlebrush conformations in the bulk because the surrounding linear matrix introduced potential immiscibility effects with the side chains of the bottlebrush polymers. Studying a wider range of systems provides a deeper knowledge of bottlebrush behavior within other relevant environments. For example, many applications rely on solution-based casting methods, where the addition of solvent is likely to affect chain behavior. In many processes involving solution-based casting, materials transition from dilute to concentrated solutions and then to the solid state, so studying the behavior at these intermediate junctions is highly relevant to understanding their final morphology.[24,25] Additionally, bottlebrushes within a linear matrix insufficiently capture behavior within many applications, where materials are often entirely composed of bottlebrush polymers.[6,26] There are numerous theoretical studies that dive into the question of chain behavior in bottlebrush melts,[27–29] but currently there is a deficit of experimental techniques to explore similar systems. Diversifying the systems studied by SMLM is attractive because there is interest in understanding their behavior in many other application-relevant environments.

In this work, we focus on the effects of changing the environments around bottlebrush polymers and compare these results to those of our previous studies on linear matrices. We first investigated bottlebrush conformations within linear matrices swollen by a good solvent. These solvent-swollen systems are analogous to concentrated polymer solutions. We also studied the conformation of bottlebrush polymers within a bottlebrush matrix. Studying these systems significantly builds upon our earlier work by reducing the immiscibility effects previously observed between linear and bottlebrush polymers. Furthermore, it expands the scope to more application-relevant systems that rely on bulk or crowded environments.

Methods and materials

All materials were acquired from Sigma-Aldrich unless otherwise stated. Bottlebrush polymers were synthesized using previously published methods that used a grafting-from approach.[30–32] Poly(hydroxyl-ethylmethacrylate) (Polymer Source, M_n = 245.6 kg mol^{-1}, $Đ$ = 1.19) (PHEMA) was functionalized by coupling with α-bromoisobutyryl bromide to form poly(2-(2-bromoisobutyryloxy)ethyl methacrylate) (PBIEM). The dye-labeled species were synthesized and characterized in a past study.[23] Unlabeled bottlebrush polymers for the polymer matrices of melts were synthesized using the same method. The characterization of the side chain molecular weight of the matrix polymers was performed by gel permeation chromatography (GPC) using an Agilent 1260 Infinity II system equipped with two columns in series (PLgel MIXED-B LS, 7.5 × 300 mm^2, 10 μm) and a light scattering detector (Wyatt Dawn 8) operated with chloroform. The dn/dc value used for PMMA in chloroform was determined to be 0.065 mL g^{-1}. The side chain molecular weight was determined by cleaving the side chains from the backbone by methanolysis and characterized using the same GPC procedure as mentioned above.[23]

Polymer film samples were prepared by spin coating solutions composed of 1 wt% polymer in anisole, where the polymer was a 0.03 : 1 mixture of a dye-labeled polymer to an unlabeled polymer by weight. For films used in the solvent swelling experiments, the unlabeled polymer was a 350 000 g mol^{-1} linear PMMA. The synthesized bottlebrush polymers were used as the matrices for the bottlebrush melt samples. All films were prepared on Piranha-treated #1.5 thickness coverslips by spin coating at 800 RPM for 10 seconds and then 3000 RPM for 1 minute to produce 40 nm thick films.

SMLM experiments on polymer films were performed using the same optical setup as reported previously.[23,31] This setup features a custom modified Olympus IX73 inverted microscope equipped with optical components from ThorLabs. All super-resolution images were composed of 10 000 frames taken at 10 ms exposure times. Super-resolution images were analyzed using the image processing toolbox in MATLAB to trace a central line through relevant features, determining a tangent–tangent correlation function $C(s)$ from these traces, and extracting a persistence length value by fitting the ensemble-average $C(s)$ to an exponential decay. These methods are described in greater detail in earlier work.[23]

Solvent experiments were performed by using a custom-built sample chamber with an inlet for solvent vapor (Fig. S1a†). The amount of solvent within the system was controlled by two mass flow controllers (MFCs) (Alicat MCS-100SCCM-D/5M). One MFC bubbled nitrogen gas through toluene, while the other streamed it directly into the chamber at a total flow rate of 100 sccm (Fig. S1b and c†). The ratio between the two flows enabled control of the toluene vapor pressure within the chamber. During *in situ* imaging experiments, the flow rates on the MFCs were kept constant for two hours before imaging under each solvent condition to ensure that the sample reached an equilibrium swelling con-

dition. The conditions used ranged from 30 to 70% of the saturated toluene stream, resulting in swelling ratios between 5 and 30%. The swelling ratio is defined as the fractional mass increase relative to the original mass of the dry film, given by,

$$\text{Swelling ratio} = \frac{W_s - W_i}{W_i} \quad (1)$$

where W_s is the weight of the swollen film and W_i is the weight of the dry film before swelling. The swelling ratio was later confirmed using a quartz crystal microbalance (QCM) (Advanced Wave Sensors, Valencia, Spain) with an N2PK impedance analyzer (Thornhill, Canada), equipped with a near-identical solvent setup. More on QCM measurements can be found in section 3 of the ESI.†

Results and discussion

To study the effects of the local environment on the conformation and behavior of bottlebrush polymers, we designed a set of single-molecule localization microscopy (SMLM) imaging experiments on bottlebrushes within linear matrices swollen with solvent and within materials entirely composed of bottlebrush polymers. For these studies, we revisit the fluorescently labeled bottlebrush polymers previously reported and investigated in earlier SMLM studies (Table 1).[23] These polymers were prepared using a grafting-from approach, beginning with a poly(2-(2-bromoisobutyryloxy)ethyl methacrylate) (PBIEM) backbone and polymerizing poly(methyl methacrylate) (PMMA) side chains directly from the backbone. These polymers were prepared such that each backbone BIEM repeat unit is expected to have one side chain. By using the same set of polymers here as in our previous study, we can make direct comparisons between the originally investigated hybrid system and the solvent-swollen system and the bottlebrush melt system discussed in this work.

Table 1 Molecular weight of bottlebrush polymers

M_{sc} (g mol^{-1})	Fluorescent labeling[a]	$Đ_{sc}$	M_{bb}, theoretical[b] (kg mol^{-1})
640	Labeled	1.10	1380
1100	Labeled	1.31	2240
2030	Labeled	1.22	3980
2860	Labeled	1.22	5540
3500	Labeled	1.27	6730
750	Unlabeled	1.36	1580
1000	Unlabeled	1.23	2050
2100	Unlabeled	1.58	4110
2700	Unlabeled	1.82	5230
4020	Unlabeled	1.23	7700

[a] The labeled bottlebrushes in this table were synthesized for a previous study and studied again here. The unlabeled bottlebrushes were synthesized for this study. [b] The theoretical molecular weight of the full bottlebrush is used as an approximation for comparison. In actuality, the molecular weight is closer to approximately 90% of this value based on our previous measurements.[23]

In order to test the local environment effects on bottlebrush conformations, we swelled toluene into polymer films composed of bottlebrushes in a linear matrix. We imaged the five dye-labeled PMMA bottlebrush polymers with different side chain molecular weights (M_{sc}) in linear matrices composed of PMMA (350 000 g mol^{-1}) (Fig. 1) in 40 nm thick polymer films. This thickness is convenient because it easily falls within the depth of the field of our microscope objective, so 3D conformations can be projected onto 2D images. Additionally, because 40 nm is an order of magnitude larger than the expected R_g of the side chains, their behavior should unaffected by confinement effects. Since the backbone conformation is driven by the behavior of the side chains, confinement is thus expected to have negligible effects on the bottlebrushes. In our previous work, we also confirmed that confinement has a minimal effect on the backbone conformation, using Monte Carlo simulations, showing that our established analysis methods can accurately determine a persistence length value from simulated chains in a confined film.[23] Each film was prepared by spin coating and annealed for 2 hours under nitrogen at 180 °C. For each of the five M_{sc} conditions, the films were swollen by 70% saturated toluene vapor *in situ* for two hours using a custom sample chamber mounted directly on the microscope (see the ESI, Fig. S1†), resulting in an equilibrium swelling ratio of 0.20. This degree of swelling is not expected to drastically increase the thickness of the sample beyond 20% of the original thickness. The swelling ratio was determined *ex situ* on films using a quartz crystal microbalance (QCM) in a similar solvent vapor setup (see the ESI†). Attempts to achieve swelling ratios above 0.20 resulted in large fluctuations in the measured mass, thus rendering the data unreliable. From these images, we determined the ensemble-averaged persistence length (l_p) for each M_{sc} condition from the tangent–tangent correlation function of the skeletonized trace of the feature. Further details of this analysis are discussed in our previous work.[23] The persistence length results are summarized in Fig. 2. We observe a decrease in l_p for each of these M_{sc} conditions from non-swollen to swollen systems. Additionally, we observe a minimal change in the scaling relationship between l_p and M_{sc}. However, because of the large uncertainties in our determined l_p values and only a few data points that do not span a wide range, we are cautious about extracting definitive conclusions from these scaling exponents.

To further probe the effects of solvent on bottlebrush conformations within linear matrices, we also explored different swelling ratios under the same M_{sc} conditions. Here, we imaged a bottlebrush polymer with an M_{sc} of 3500 g mol^{-1} within a linear matrix at swelling ratios of 0–20% toluene. The lowest swelling condition of 5% was set by the lowest solvent vapor saturation of 30% to produce a mass increase discernible from noise. Each condition was held for two hours before imaging to ensure equilibrium conditions. We observed a relatively high persistence length of 290 nm under the no solvent condition, which decreased sharply to 250 nm upon swelling to only 5% (Fig. 3). Upon further swelling, the l_p quickly

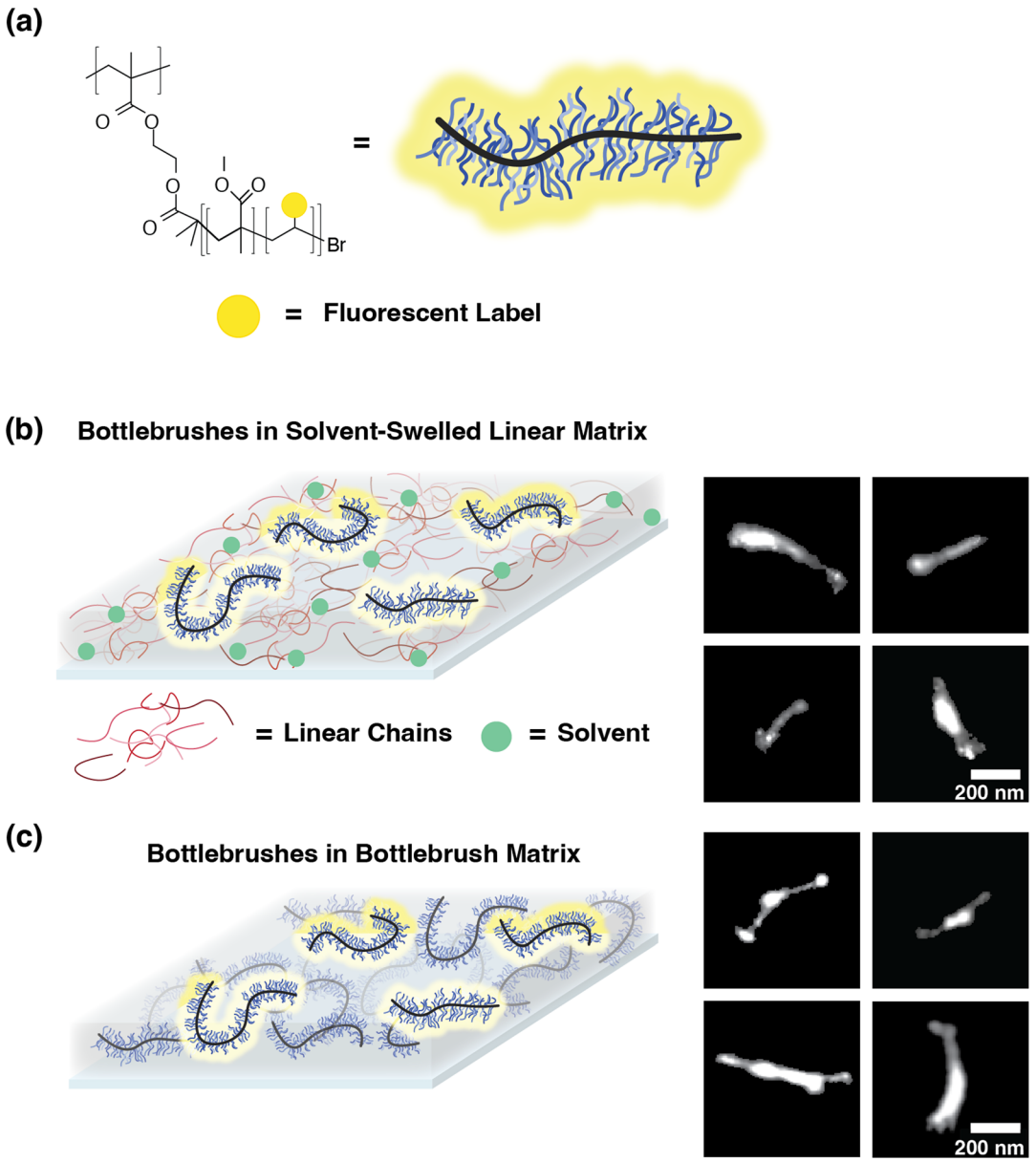

Fig. 1 (a) Structure of bottlebrush polymers composed of PMMA side chains and a PBIEM backbone. The fluorescent label is a photoswitchable diarylethene as previously reported.[31,33] (b and c) Schematic and representative features within solvent-swollen linear–bottlebrush hybrid systems and bottlebrush melts. (b) A linear matrix swollen with solvent with a dilute amount of labeled bottlebrushes dispersed, with features depicting single bottlebrush chains (M_{sc} = 3500 g mol^{-1}). (c) Bottlebrush polymers within a bottlebrush matrix, with features depicting single bottlebrush chains (M_{sc} = 3500 g mol^{-1}).

reached a plateau value of approximately 230 nm. It is rather surprising that only a small amount of solvent in the environment has a large effect on the conformation. Perhaps this demonstrates a hard threshold between a highly concentrated regime and the neat polymer, where the presence of the solvent at even low concentrations already has an impact on the physics affecting the system.

Based on the difference in the persistence lengths between non-swollen and swollen polymer films, our SMLM experiments suggest that the presence of solvent promotes chain flexibility. This phenomenon can be explained by considering the effects of solvent on the side chains, which largely drive the conformation behavior of the bottlebrush backbone. In our previous work, we hypothesized that autophobic dewetting largely affects the behavior of side chains, which in turn drives the conformation of the entire bottlebrush.[23] Autophobic dewetting occurs in systems with short grafted chains and long matrix chains of the same chemical identity because it is entropically unfavorable for the matrix chains to interpenetrate into the pervaded volume of the grafted chains.[34] Instead, there are more overall configurations if the grafted chains collapse to a smaller space and the matrix chains occupy the

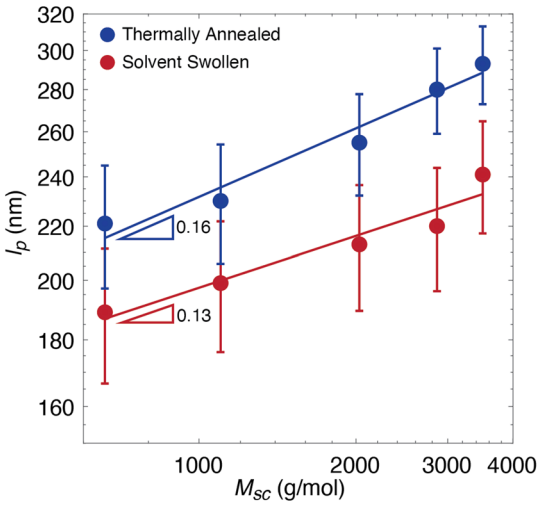

Fig. 2 Persistence lengths of PMMA bottlebrush polymers in non-swollen and 20% toluene-swollen linear PMMA films as a function of side chain molecular weight. Each data point consists of 350 chains. Error bars are 90% confidence intervals, which were determined by calculating the standard deviation in l_p based on 10 sets of 350 wormlike chains from simulations (see previous work for details).[22,23] Lines represent power law fits. Due to uncertainties in our technique, we are less confident about lower l_p values. Fitting the highest three points of the solvent-swollen series results in a scaling exponent of 0.22. Note that the data span less than one decade in the abscissa, so we encourage caution in interpreting the power law fit in general.

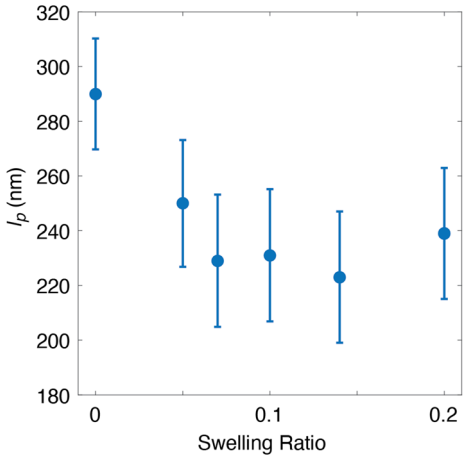

Fig. 3 Persistence lengths of PMMA bottlebrush polymers in linear–bottlebrush hybrid systems at various swelling ratios of toluene (eqn (1)). The M_{sc} of the bottlebrush polymer was 3500 g mol^{-1}. Each data point consists of 350 chains. Error bars are the 90% confidence intervals, based on the 10 sets of 350 wormlike chains from simulations.

resulting larger separate space. This causes the side chains to behave as hard spheres rather than Gaussian chains, which increases backbone rigidity due to higher degrees of steric repulsion from the bulky groups close to the backbone.

Here, we introduced a good solvent into the local environment surrounding the bottlebrushes, which may relax the side chains from collapsed spheres to swollen coils. This change in behavior drives the overall flexibility of the backbone. The radius of gyration for coils scales as $R_g \sim N^{1/2}$ and for collapsed spheres as $R_g \sim N^{1/3}$, where N is the number of repeat units on the chain and is equivalent to M_{sc} here. Based on theory, the persistence length of a bottlebrush in a melt is expected to scale as the size of the side chains, with $l_p \sim R_g$.[27] However, to our knowledge there is no study in the literature that specifically relates M_{sc} to l_p under the effect of solvent swelling, and so we propose an explanation for our results here. Although coils are expected to be larger because they are swollen, they are no longer hard spheres and thus their pervaded volumes should easily interpenetrate into each other and with the matrix chains, which decreases steric effects on the backbone and promotes chain flexibility of the entire molecule (Fig. 4).

Although this proposed mechanism offers a simple explanation for the change in persistence length with respect to solvent swelling, it does not explain the change in the scaling relationship between l_p and M_{sc}. Because we expect the backbone conformation to be driven by the behavior of the side chains as previously hypothesized,[27] we would expect a change in the scaling behavior in addition to the change in rigidity discussed previously. However, we do not observe a significant change in the scaling exponent. While we are cautious to make conclusions on the scaling behavior due to the large uncertainties in l_p values and the limited less-than-one-decade range over which our data span, one would expect some variation to reflect the change in the environment. The failure to observe this variation may be an artifact because we are close to the resolution limit of our SMLM imaging technique. As discussed in our previous study, super-resolution microscopy has an implicit resolution limit that affects the accuracy of localizing the fluorescent labels on the bottlebrush. This introduces an uncertainty in fitting the bottlebrush images and extracting an accurate l_p value. From our analysis, we found that this accuracy decreases for l_p values below 200 nm.[23] Therefore, the persistence lengths determined for the lower M_{sc} conditions are less reliable, and this may explain the discrepancy when comparing our results to the theoretically expected scaling relationship. Because our analysis tool often overestimates l_p under these conditions, a higher scaling exponent would be expected if this resolution limit were not present. Excluding the lowest two points leads to a scaling exponent of 0.22. However, because of the inherent uncertainties, it is difficult to make a strong assertion from this result. Nevertheless, we do observe a consistent and reliable decrease in persistence length for many of the M_{sc} conditions, so we assert that the solvent has an effect in promoting chain flexibility.

Despite being close to the resolution limit of our technique and facing difficulty resolving the entire contour of the bottlebrush chains, we do observe a qualitative difference in the features between non-swollen and swollen films (Fig. 5a). For conditions with shorter side chains (M_{sc} = 640 and 1100 g mol^{-1}), we observe many more coiled features and fewer rod-like features than we would typically expect. These features are much larger than the artifacts that arise from fluorescent impurities,

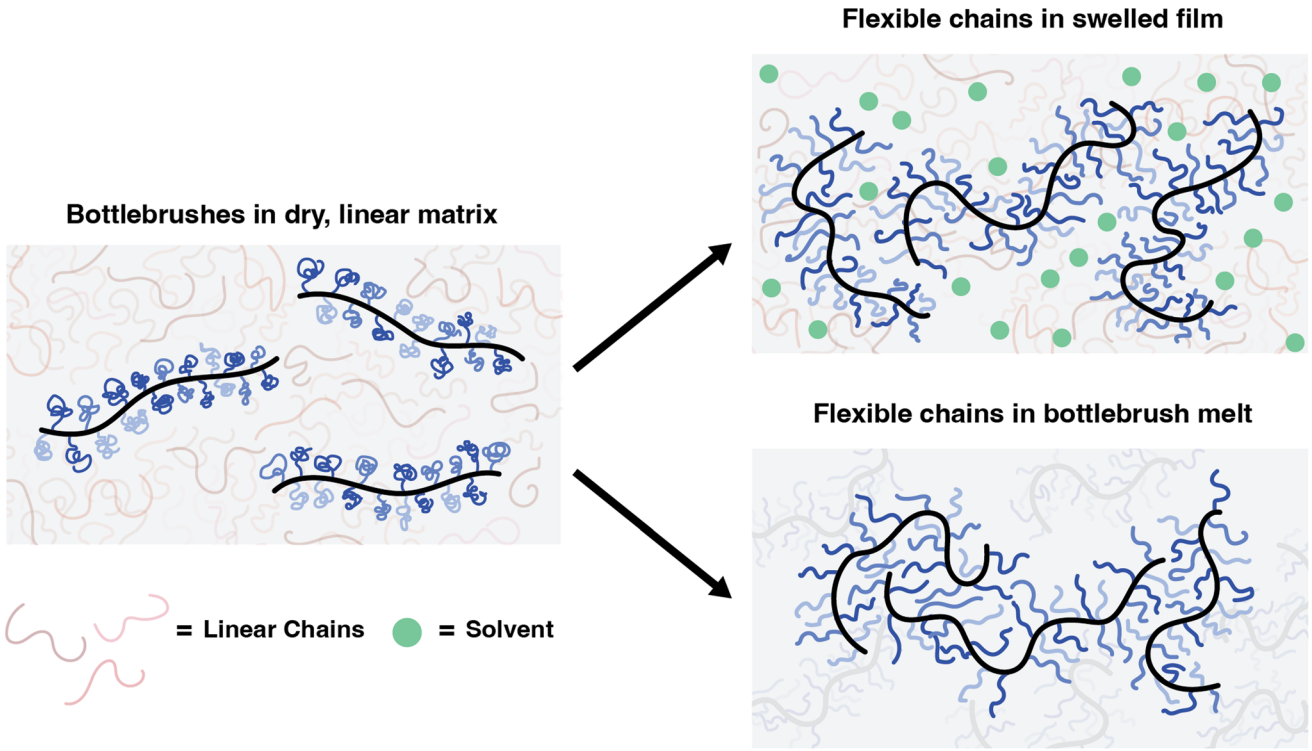

Fig. 4 Schematic depicting the effects of autophobic dewetting on the bottlebrush conformation. In a dry film composed of a linear chain matrix, the bottlebrush polymers are rigid due to their collapsed side chains. The addition of solvent relaxes the side chains, and the conformation of the bottlebrushes becomes more flexible. In a bottlebrush melt, where no autophobic dewetting effects occur, the side chains outstretch, penetrating the pervaded volumes of neighboring chains, allowing them to conform around one another.

which are generally less than 100 nm in size. Because of this, we suspect that we are instead observing the effects of the solvent increasing chain flexibility to such a degree that they no longer appear elongated. We test this theory by studying the aspect ratio of the features found in these swelling experiments. Here, we define an aspect ratio as a ratio between the major and minor axes of an ellipse fit to the feature (Fig. 5b), derived from the eigenvalues of the covariance matrix of the positions of the fluorophore localization events in the SMLM experiment. From this ratio, we can quantify the shape of each feature, where a lower value indicates a more coiled conformation and a higher value indicates a more rod-like conformation. Prior to swelling with the solvent, we observe a greater population of higher aspect ratio features (Fig. 5c). Additionally, we compared two different M_{sc} conditions (M_{sc} = 640 and 3500) that were swollen with toluene at a 20% swelling ratio, which shows that this aspect ratio also decreases with M_{sc}. Therefore, these results suggest that for lower M_{sc} conditions only, the solvent induces flexibility to such an extent that the entire contour is no longer visible with our SMLM resolution capabilities. As we reach this limit, we can no longer reliably determine the persistence lengths, resulting in large uncertainties and scaling relationships that deviate significantly from theory. Although the resolution limits of our technique result in these uncertainties, the aspect ratio analysis provides additional confidence that solvent swelling indeed increases backbone flexibility, consistent with the mechanism of reduced autophobic dewetting.

While ideally an even more powerful experiment would track the exact same chains under different solvent swelling conditions, we do not currently have the technical capabilities to perform such experiments. One of the challenges that limits our abilities is the lifetime of the dye under photobleaching conditions. Currently, it is difficult to perform long time-lapse experiments because as dyes photobleach, the quality of the resulting super-resolution image drops. Additionally, chains are expected to migrate and undergo conformational changes as a result of solvent swelling. Compounded with sample drift and photobleaching, this makes it difficult to ensure that features observed early in acquisition are the same as those observed later in an *in situ* experiment. We therefore rely on analyses that average over a large ensemble to make conclusions on the effects of solvent swelling.

To further explore the effect of the surrounding environment on bottlebrush conformations, we studied systems where the matrix is entirely composed of bottlebrushes. In these systems, autophobic dewetting is not expected to occur at all because there are no large molecular weight differences between the side chains of neighboring bottlebrushes. We synthesized five different bottlebrush polymers containing no

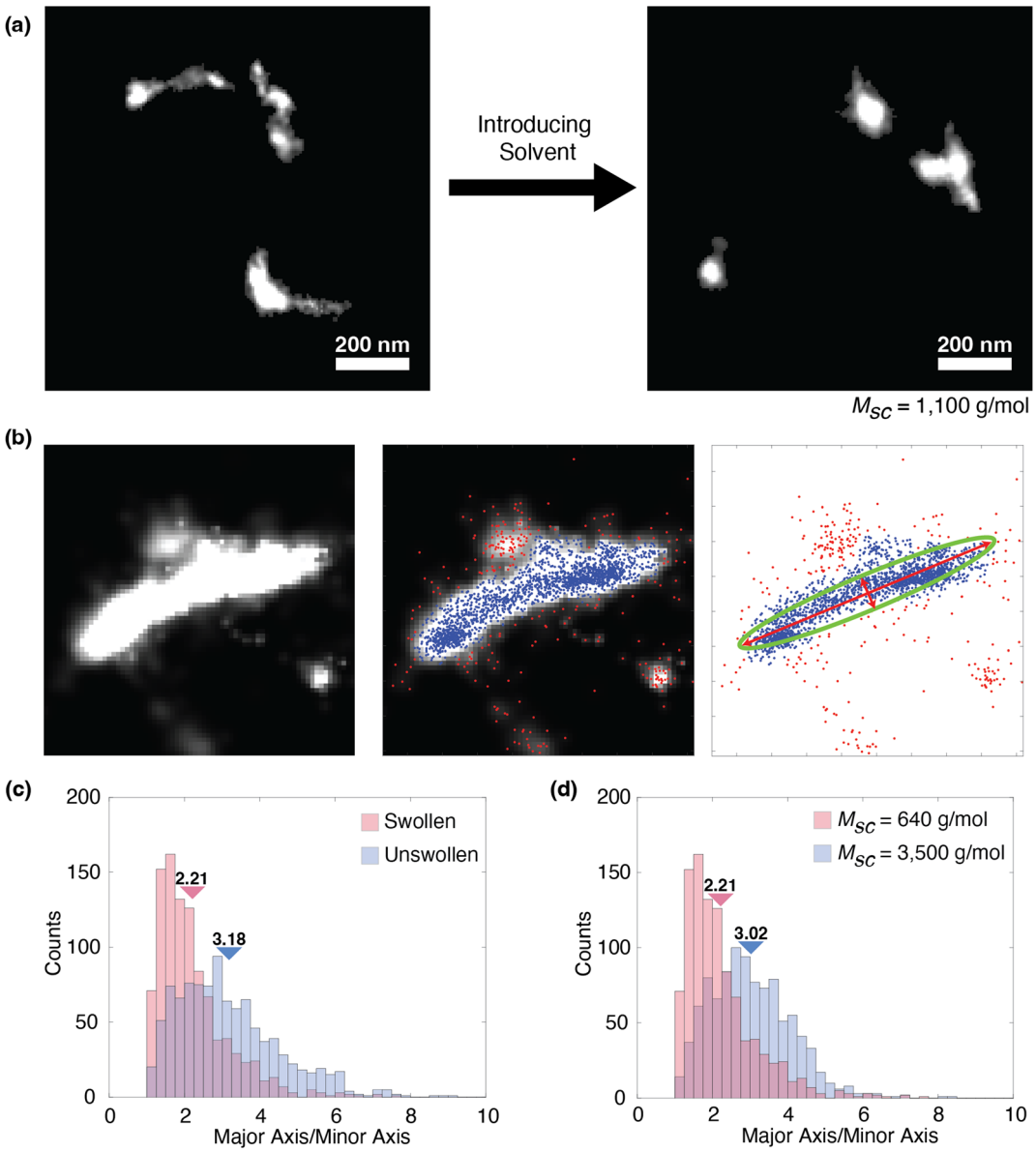

Fig. 5 (a) Representative data showing solvent effects on low M_{sc} conditions. Bottlebrushes here have M_{sc} = 1100 g mol^{-1}. The two images show different regions within the same sample before and after swelling with the solvent, but they do not show the same bottlebrushes. (b) Schematic determining the major and minor axes from super-resolution images. (From left to right) The first panel shows the super-resolution image of a single bottlebrush feature. The second panel is the same image with the localizations superimposed on top. The blue dots represent localizations that fall within the pixels belonging to the bottlebrush feature, which is determined by our analysis procedure. Red dots are localizations that fall outside of this feature. This process is described in more detail in our previous work.[23] The third panel displays only the localizations with the fitted ellipse plotted over the points. The red arrows represent the major and minor axes of the ellipse. (c) Histogram of the aspect ratios from swollen (at a 20% swelling ratio) and unswollen samples. These data reflect the same sample, where M_{sc} = 640 g mol^{-1}. Each condition consists of 1000 features. Triangles indicate the mean of each condition (2.21 for swollen and 3.18 for unswollen). (d) Histogram of the aspect ratios of two different swollen samples with different side chain lengths. Both conditions involve swelling at a 20% swelling ratio. Each condition consists of 1000 features. Triangles indicate the mean of each condition (2.21 for 640 g mol^{-1} and 3.02 for the unswollen sample at 3500 g mol^{-1}).

fluorescent labels for the matrix of these samples, each matching one of the five dye-labeled bottlebrush polymers previously used (Table 1). Each labeled system was blended with its corresponding unlabeled matrix and persistence lengths were extracted using the same methods as previously discussed (Fig. 6). The persistence lengths decreased for each of the melt systems compared to those previously reported for linear matrices. Additionally, the l_p *vs.* M_{sc} scaling exponent appears to increase from 0.16 to 0.39, though we caution the reader about overinterpretation similar to that mentioned above, due to the relatively large uncertainties and small span of the data.

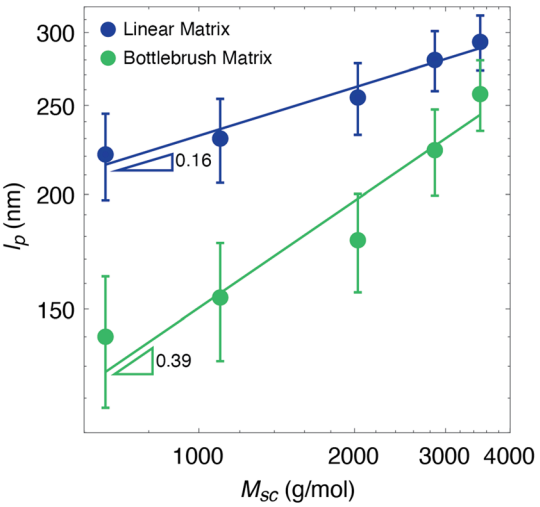

Fig. 6 Persistence lengths of bottlebrush polymers in linear and bottlebrush matrices with respect to side chain molecular weight. The linear matrix data are identical to Fig. 2. Each data point is based on 350 chains. Error bars are the 90% confidence intervals, based on 10 sets of 350 simulated wormlike chains. Lines represent a power law fit. Due to uncertainties in our technique, we are less confident about lower l_p values. Fitting the highest four points of the bottlebrush matrix series results in a scaling exponent of 0.47. Note that the data span less than one decade in the abscissa, so we encourage caution in interpreting the power law fit in general.

When transitioning from a linear to a bottlebrush matrix, the decrease in persistence lengths and the increase in l_p *vs.* M_{sc} scaling are consistent with the removal of autophobic dewetting effects. In a matrix composed of bottlebrushes rather than linear polymers, there is no large molecular weight mismatch, and the number of configurations is not reduced when the side chains interpenetrate with those of neighboring bottlebrushes (Fig. 4). Therefore, there is no entropic penalty for the side chains to behave as Gaussian chains, leading to much greater backbone flexibility. This is reflected in our extracted l_p values, where we observe a decrease for each of the M_{sc} conditions. Additionally, the scaling exponent of 0.39 is closer to the expected value of 0.5 for bottlebrush melts, which has been reported in various theoretical studies.[27–29] As previously discussed, because of the resolution limitations of our super-resolution imaging and analysis tool, the lower extracted persistence length values at the lowest M_{sc} conditions are potentially overestimations of the true value. Eliminating the lowest data point leads to a scaling exponent of 0.47. However, because we are near this resolution limit, we are cautious to extract definitive conclusions on the scaling behavior. The overall trends observed here do provide some evidence that bottlebrushes within a bottlebrush matrix deviate from those within a linear matrix, where autophobic dewetting effects may largely drive the behavior. Overall, the increased flexibility and scaling behavior observed through these SMLM experiments are consistent with explanations proposed for our previous work and with theoretical studies on bottlebrush melts.

Conclusion

In this work, we expanded on our previous investigations using SMLM to study the single chain conformations of bottlebrush polymers, aiming to understand the effect of the changes in local environments around the bottlebrush on chain rigidity. From our previous experiments, we hypothesized that autophobic dewetting in linear–bottlebrush hybrid systems led to highly rigid bottlebrushes that diverged greatly from expected behaviors based on theory. Here, we introduced conditions that opposed these entropic effects and reduced autophobic dewetting. Although we observed more flexible chains within these solvent-swollen systems, the expected scaling behavior between l_p and M_{sc} did not precisely align with our expectations, which may be due to the resolution limit of our imaging technique. We additionally investigated neat systems entirely composed of bottlebrush polymers. Here, we also observed greater flexibility and a scaling relationship closer to theoretical predictions. Despite working close to the SMLM resolution limit, our results indicate a change in the scaling relationship that more closely resembles theoretical studies on similar systems. Overall, expanding on our SMLM experiments provides evidence that the local environment plays a significant role in the chain conformation, further supporting our previous theories that autophobic dewetting significantly affects bottlebrush rigidity.

Conflicts of interest

There are no conflicts to declare.

Acknowledgements

The authors acknowledge Profs. Julia Kalow and John Torkelson for access to equipment and useful discussions, and funding from the National Science Foundation (DMR-1945249) for support of this work. M. W. acknowledges support from the Alfred P. Sloan Foundation and The Camille and Henry Dreyfus Foundation. This work made use of the Integrated Molecular Structure Education and Research Center (IMSERC) facility at Northwestern University, which has received support from the Soft and Hybrid Nanotechnology Experimental Resource (NSF ECCS-2025633), the State of Illinois, and the International Institute for Nanotechnology.

References

1 X. Yin, Y. Qiao, M. R. Gadinski, Q. Wang and C. Tang, Flexible Thiophene Polymers: A Concerted Macromolecular Architecture for Dielectrics, *Polym. Chem.*, 2016, 7(17), 2929–2933, DOI: 10.1039/c6py00233a.
2 C. M. Tonge, E. R. Sauvé, S. Cheng, T. A. Howard and Z. M. Hudson, Multiblock Bottlebrush Nanofibers from

Organic Electronic Materials, *J. Am. Chem. Soc.*, 2018, **140**(37), 11599–11603, DOI: 10.1021/jacs.8b07915.

3 M. Vatankhah-Varnosfaderani, A. N. Keith, Y. Cong, H. Liang, M. Rosenthal, M. Sztucki, C. Clair, S. Magonov, D. A. Ivanov, A. V. Dobrynin and S. S. Sheiko, Chameleon-like Elastomers with Molecularly Encoded Strain-Adaptive Stiffening and Coloration, *Science*, 2018, **359**(6383), 1509–1513, DOI: 10.1126/science.aar5308.

4 A. N. Keith, M. Vatankhah-Varnosfaderani, C. Clair, F. Fahimipour, E. Dashtimoghadam, A. Lallam, M. Sztucki, D. A. Ivanov, H. Liang, A. V. Dobrynin and S. S. Sheiko, Bottlebrush Bridge between Soft Gels and Firm Tissues, *ACS Cent. Sci.*, 2020, **6**(3), 413–419, DOI: 10.1021/acscentsci.9b01216.

5 W. F. M. Daniel, J. Burdyńska, M. Vatankhah-Varnoosfaderani, K. Matyjaszewski, J. Paturej, M. Rubinstein, A. V. Dobrynin and S. S. Sheiko, Solvent-Free, Supersoft and Superelastic Bottlebrush Melts and Networks, *Nat. Mater.*, 2016, **15**(2), 183–189, DOI: 10.1038/nmat4508.

6 M. Vatankhah-Varnosfaderani, W. F. M. Daniel, M. H. Everhart, A. A. Pandya, H. Liang, K. Matyjaszewski, A. V. Dobrynin and S. S. Sheiko, Mimicking Biological Stress-Strain Behaviour with Synthetic Elastomers, *Nature*, 2017, **549**(7673), 497–501, DOI: 10.1038/nature23673.

7 B. B. Patel, D. J. Walsh, D. H. Kim, J. Kwok, B. Lee, D. Guironnet and Y. Diao, Tunable Structural Color of Bottlebrush Block Copolymers through Direct-Write 3D Printing from Solution, *Sci. Adv.*, 2020, **6**(24), eaaz7202, DOI: 10.1126/sciadv.aaz7202.

8 R. Xie, S. Mukherjee, A. E. Levi, V. G. Reynolds, H. Wang, M. L. Chabinyc and C. M. Bates, Room Temperature 3D Printing of Super-Soft and Solvent-Free Elastomers, *Sci. Adv.*, 2020, **6**(46), 1–11, DOI: 10.1126/sciadv.abc6900.

9 J. L. Self, C. S. Sample, A. E. Levi, K. Li, R. Xie, J. R. De Alaniz and C. M. Bates, Dynamic Bottlebrush Polymer Networks: Self-Healing in Super-Soft Materials, *J. Am. Chem. Soc.*, 2020, **142**(16), 7567–7573, DOI: 10.1021/jacs.0c01467.

10 D. F. Sunday, A. Chremos, T. B. Martin, A. B. Chang, A. B. Burns and R. H. Grubbs, Concentration Dependence of the Size and Symmetry of a Bottlebrush Polymer in a Good Solvent, *Macromolecules*, 2020, **53**(16), 7132–7140, DOI: 10.1021/acs.macromol.0c01181.

11 C. R. López-Barrón and M. E. Shivokhin, Extensional Strain Hardening in Highly Entangled Molecular Bottlebrushes, *Phys. Rev. Lett.*, 2019, **122**(3), 37801, DOI: 10.1103/PhysRevLett.122.037801.

12 C. R. López-Barrón, A. H. Tsou, J. R. Hagadorn and J. A. Throckmorton, Highly Entangled α - Olefin Molecular Bottlebrushes: Melt Structure, Linear Rheology, and Interchain Friction Mechanism, *Macromolecules*, 2018, **51**(17), 6958–6966, DOI: 10.1021/acs.macromol.8b01431.

13 S. J. Dalsin, M. A. Hillmyer and F. S. Bates, Linear Rheology of Polyolefin-Based Bottlebrush Polymers, *Macromolecules*, 2015, **48**(13), 4680–4691, DOI: 10.1021/acs.macromol.5b01153.

14 I. N. Haugan, M. J. Maher, A. B. Chang, T. P. Lin, R. H. Grubbs, M. A. Hillmyer and F. S. Bates, Consequences of Grafting Density on the Linear Viscoelastic Behavior of Graft Polymers, *ACS Macro Lett.*, 2018, **7**(5), 525–530, DOI: 10.1021/acsmacrolett.8b00116.

15 S. L. Pesek, X. Li, B. Hammouda, K. Hong and R. Verduzco, Small-Angle Neutron Scattering Analysis of Bottlebrush Polymers Prepared via Grafting-through Polymerization, *Macromolecules*, 2013, **46**(17), 6998–7005, DOI: 10.1021/ma401246b.

16 S. L. Pesek, Q. Xiang, B. Hammouda and R. Verduzco, Small-Angle Neutron Scattering Analysis of Bottlebrush Backbone and Side Chain Flexibility, *J. Polym. Sci., Part B: Polym. Phys.*, 2017, **55**(1), 104–111, DOI: 10.1002/polb.24251.

17 D. F. Sunday, A. B. Chang, C. D. Liman, E. Gann, D. M. Delongchamp, L. Thomsen, M. W. Matsen, R. H. Grubbs and C. L. Soles, Self-Assembly of ABC Bottlebrush Triblock Terpolymers with Evidence for Looped Backbone Conformations, *Macromolecules*, 2018, **51**(18), 7178–7185, DOI: 10.1021/acs.macromol.8b01370.

18 S. J. Dalsin, T. G. Rions-Maehren, M. D. Beam, F. S. Bates, M. A. Hillmyer and M. W. Matsen, Bottlebrush Block Polymers: Quantitative Theory and Experiments, *ACS Nano*, 2015, **9**(12), 12233–12245, DOI: 10.1021/acsnano.5b05473.

19 N. Borodinov, A. Belianinov, D. Chang, J. M. Carrillo, M. J. Burch, Y. Xu, K. Hong, A. V. Ievlev, B. G. Sumpter and O. S. Ovchinnikova, Molecular Reorganization in Bulk Bottlebrush Polymers: Direct Observation: Via Nanoscale Imaging, *Nanoscale*, 2018, **10**(37), 18001–18009, DOI: 10.1039/c8nr05630g.

20 M. A. Thompson, M. D. Lew and W. E. Moerner, Extending Microscopic Resolution with Single-Molecule Imaging and Active Control, *Annu. Rev. Biophys.*, 2012, **41**(1), 321–342, DOI: 10.1146/annurev-biophys-050511-102250.

21 Z. Qiang and M. Wang, 100th Anniversary of Macromolecular Science Viewpoint: Enabling Advances in Fluorescence Microscopy Techniques, *ACS Macro Lett.*, 2020, **9**(9), 1342–1356, DOI: 10.1021/acsmacrolett.0c00506.

22 J. M. Chan and M. Wang, Visualizing the Orientation of Single Polymers Induced by Spin-Coating, *Nano Lett.*, 2022, **22**(14), 5891–5897, DOI: 10.1021/acs.nanolett.2c01830.

23 J. M. Chan, A. C. Kordon, R. Zhang and M. Wang, Direct Visualization of Bottlebrush Polymer Conformations in the Solid State, *Proc. Natl. Acad. Sci. U. S. A.*, 2021, **118**(40), 1–9, DOI: 10.1073/pnas.2109534118.

24 B. R. Sveinbjornsson, R. A. Weitekamp, G. M. Miyake, Y. Xia, H. A. Atwater and R. H. Grubbs, Rapid Self-Assembly of Brush Block Copolymers to Photonic Crystals, *Proc. Natl. Acad. Sci. U. S. A.*, 2012, **109**(36), 14332–14336, DOI: 10.1073/pnas.1213055109.

25 D. P. Song, T. H. Zhao, G. Guidetti, S. Vignolini and R. M. Parker, Hierarchical Photonic Pigments via the Confined Self-Assembly of Bottlebrush Block Copolymers, *ACS Nano*, 2019, **13**(2), 1764–1771, DOI: 10.1021/acsnano.8b07845.

26 W. F. M. Daniel, J. Burdyńska, M. Vatankhah-Varnoosfaderani, K. Matyjaszewski, J. Paturej, M. Rubinstein, A. V. Dobrynin and S. S. Sheiko, Solvent-Free, Supersoft and Superelastic Bottlebrush Melts and Networks, *Nat. Mater.*, 2016, **15**(2), 183–189, DOI: **10.1038/nmat4508**.

27 J. Paturej, S. S. Sheiko, S. Panyukov and M. Rubinstein, Molecular Structure of Bottlebrush Polymers in Melts, *Sci. Adv.*, 2016, **2**(11), e1601478, DOI: **10.1126/sciadv.1601478**.

28 H. Liang, Z. Cao, Z. Wang, S. S. Sheiko and A. V. Dobrynin, Combs and Bottlebrushes in a Melt, *Macromolecules*, 2017, **50**(8), 3430–3437, DOI: **10.1021/acs.macromol.7b00364**.

29 H. Liang, Z. Wang, S. S. Sheiko and A. V. Dobrynin, Comb and Bottlebrush Graft Copolymers in a Melt, *Macromolecules*, 2019, **52**(10), 3942–3950, DOI: **10.1021/acs.macromol.9b00611**.

30 J. Rzayev, Synthesis of Polystyrene-Polylactide Bottlebrush Block Copolymers and Their Melt Self-Assembly into Large Domain Nanostructures, *Macromolecules*, 2009, **42**(6), 2135–2141, DOI: **10.1021/ma802304y**.

31 Z. Qiang, K. M. Shebek, M. Irie and M. Wang, A Polymerizable Photoswitchable Fluorophore for Super-Resolution Imaging of Polymer Self-Assembly and Dynamics, *ACS Macro Lett.*, 2018, **7**(12), 1432–1437, DOI: **10.1021/acsmacrolett.8b00686**.

32 K. Uno, H. Niikura, M. Morimoto, Y. Ishibashi, H. Miyasaka and M. Irie, In Situ Preparation of Highly Fluorescent Dyes upon Photoirradiation, *J. Am. Chem. Soc.*, 2011, **133**(34), 13558–13564, DOI: **10.1021/ja204583e**.

33 K. Uno, H. Niikura, M. Morimoto, Y. Ishibashi, H. Miyasaka and M. Irie, In Situ Preparation of Highly Fluorescent Dyes upon Photoirradiation, *J. Am. Chem. Soc.*, 2011, **133**(34), 13558–13564, DOI: **10.1021/ja204583e**.

34 P. F. Green, The Structure of Chain End-Grafted Nanoparticle/Homopolymer Nanocomposites, *Soft Matter*, 2011, **7**(18), 7914–7926, DOI: **10.1039/c1sm05076a**.